

Trabecular coating on curved alumina substrates using a novel bioactive and strong glass-ceramic

Original

Trabecular coating on curved alumina substrates using a novel bioactive and strong glass-ceramic / Baino, Francesco; VITALE BROVARONE, Chiara. - In: BIOMEDICAL GLASSES. - ISSN 2299-3932. - ELETTRONICO. - 1:(2015), pp. 31-40. [10.1515/bglass-2015-0003]

Availability:

This version is available at: 11583/2611155 since: 2016-01-13T12:55:34Z

Publisher:

De Gruyter Open

Published

DOI:10.1515/bglass-2015-0003

Terms of use:

This article is made available under terms and conditions as specified in the corresponding bibliographic description in the repository

Publisher copyright

(Article begins on next page)

Research Article

Open Access

Francesco Baino and Chiara Vitale-Brovarone*

Trabecular coating on curved alumina substrates using a novel bioactive and strong glass-ceramic

DOI 10.1515/bglass-2015-0003

Received Feb 06, 2015; accepted Apr 07, 2015

Abstract: In the last few years, optimal fixation of orthopaedic implants evolved to preserve host bone and enhance tissue integration by surface modifications, including the use of coatings with bioactive ceramics. In this work, we fabricated a novel bone-like porous bioactive glass-ceramic coating on curved alumina substrates; good joining between the two components was possible due to the interposition of a glass-derived dense interlayer. The mechanical properties of the porous glass-ceramic, which mimics the 3-D pore architecture of cancellous bone, are adequate for load-bearing applications (compressive strength of 19 MPa and fracture energy around $6.5 \times 10^{-4} \text{ J mm}^{-3}$, with a total porosity of 62 vol.%). *In vitro* bioactive behaviour was investigated by testing the samples in simulated body fluid and by evaluating the apatite formation on the surface and pore struts of the trabecular coating, which is a key precondition for *in vivo* osteointegration. The concepts disclosed in the present study could find interesting application in the context of orthopaedic implants, with particular reference to full-ceramic acetabular cups for hip joint prosthesis.

Keywords: Bioactive glass, Coating, Scaffold, Bioceramic, Hip joint prosthesis.

1 Introduction

Bioactive glasses have been studied and proposed for more than 40 years in a variety of medical applications, including middle ear ossicle replacement, bone cements

and, generally, non-load-bearing osseous implants [1, 2]. However, their use has been limited by poor mechanical strength in tension and under cyclic loading. For applications where good mechanical properties are a goal, high-strength ceramics or metal alloys are still the materials of choice. Alumina, zirconia and composites thereof are excellent materials for the fabrication of prosthetic joint surfaces because of their high biocompatibility, wear resistance and compressive strength [3], while titanium and cobalt alloys are used for those components of the implant, such as femur stem, which require an extensive load-bearing ability [4]. In spite of these attractive properties, all these high-strength materials lack osteointegration, *i.e.* the ability to bond to living bone. Once implanted *in vivo*, alumina and metal alloys induce the formation of a non-adherent fibrous capsule at the tissue-implant interface, which could involve postoperative mobility and displacement of the prosthetic component from the correct position. Therefore, modifying the surface properties by the deposition of a coating is a valuable approach to improve osteointegration while maintaining unaltered the good mechanical properties of the prosthesis. Bioactive glasses and glass-ceramics, being known to promote a strong chemical bond with surrounding bone and to encourage positive interactions between cells and implanted device, are ideal biomaterials for the fabrication of coatings [5]. Over the years, several methods have been proposed to coat a substrate with a glass or glass-ceramic layer, such as enamelling [6], plasma spraying [7], spin coating [8], radio-frequency magnetron sputtering [9], electrophoretic deposition [10, 11] and airbrush spraying [12]. In spite of their potentiality, however, bioactive glass coatings are still rarely applied, mainly due to some concerns about their long-term durability and fate *in vivo*. This opens new prospects for the scientific research, since much still has to be done to benefit fully from bioactive glass coatings.

Coatings are usually produced as dense, pore-free glass or glass-ceramic layers; in this work, carried out in the framework of the EC-funded project MATCH (“Monoblock acetabular cup with trabecular-like coating”), novel bone-like glass-derived coatings are proposed

***Corresponding Author: Chiara Vitale-Brovarone:** Institute of Materials Physics and Engineering, Applied Science and Technology Department, Politecnico di Torino, Corso Duca degli Abruzzi 24, 10129 Torino, Italy, E-mail: chiara.vitale@polito.it, Tel.: +39 011 090 4716, Fax: +39 011 090 4624

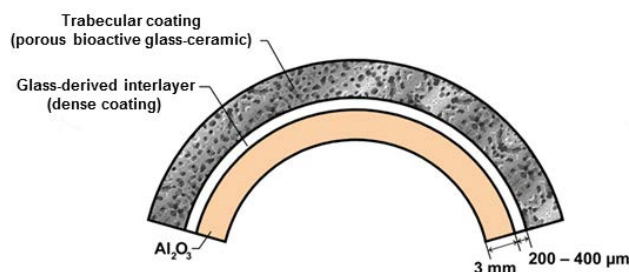
Francesco Baino: Institute of Materials Physics and Engineering, Applied Science and Technology Department, Politecnico di Torino, Corso Duca degli Abruzzi 24, 10129 Torino, Italy

 © 2015 F. Baino *et al.*, licensee De Gruyter Open.

This work is licensed under the Creative Commons Attribution-NonCommercial-NoDerivs 3.0 License.

Table 1: Starting glasses used in this work.

Glass	Oxide composition (mol.%)						Melting conditions	CTE ($\times 10^{-6} \text{ } ^\circ\text{C}^{-1}$)
	SiO ₂	CaO	Na ₂ O	Al ₂ O ₃	MgO	P ₂ O ₅		
SCNA	57	34	6	3	-	-	1550°C/1 h	8.7
S50P3	50	30	14	1	2	3	1500°C/1 h	11.3

**Figure 1:** Scheme of the novel prosthetic full-ceramic device proposed in this work.

and investigated. Our research group first claimed the concept behind this work [13], suggesting the use of a full-ceramic single-piece acetabular cup for hip joint prosthesis that could be anchored to the patient's bone without employing metal back, screws or poly(methyl methacrylate) cement but by means of a bioactive trabecular coating able to promote a "physiological" osteointegration. As schematically illustrated in Fig. 1, this new prosthetic acetabular cup is constituted by three layers: (i) an alumina substrate, (ii) a bioactive bone-like trabecular coating and (iii) a glass-derived interlayer with the aim of improving the adhesion between the bioceramic cup and the trabecular coating. New bone is expected to grow within the interconnected macroporous network of the trabecular coating. As the trabecular layer is bioactive, a tight bond between porous coating and new bone will form *in vivo*.

We recently demonstrated the feasibility of this 3-layer device in a flat geometry [14, 15]; the challenge considered in the present work is to extend these preliminary results to a more complex, curved configuration in a reproducible way, which is one of the major goals of the project MATCH.

2 Materials and methods

2.1 Starting materials

The curved ceramic substrates to be coated were obtained by cutting high-purity (> 99 wt.%) alumina crucibles in sectors (length of the external arc: 20-40 mm; external ra-

dius: 19 mm; wall thickness: 2.0 mm; width: 10 mm) using a diamond blade (330CA; Accutom 5 machine, Struers).

The compositions of the SCNA and S50P3 glasses used for the preparation of interlayer and trabecular coating are listed in Table 1. The glass reagents (high-purity oxides and carbonates, all purchased from Sigma-Aldrich) were molten in a platinum crucible in air. The melt was quenched in cold water to obtain a frit, that was then ground by a 6-ball zirconia milling machine and properly sieved below a particle size of 32 μm (stainless steel sieves, Giuliani Technologies Srl).

2.2 Dense coating (interlayer) manufacturing

We fabricated the SCNA-derived interlayer by airbrush spraying of glass suspensions; the details of the manufacturing process are reported elsewhere [12]. Briefly, a glass-based slurry (50 wt.% SCNA, 44 wt.% distilled water, 6 wt.% poly(vinyl alcohol) (PVA)) was prepared and then layer-wise deposited on the curved alumina substrates by an airbrush spray gun (Evolution Silverline M, Harder & Steenbeck, Germany). Single green layers were dried at room temperature for 1 h at the end of each spraying cycle. Once all the depositions were completed, the samples were left to dry overnight under ambient conditions; the PVA, acting as a binder, allowed manipulating these samples (with a certain caution) for the subsequent operations without damage or detachment of the green coating.

2.3 Trabecular coating fabrication

The bone-like porous coating was produced by the sponge replication method, which is recognized as one of the "gold standard" techniques to fabricate 3-D scaffolds [16–18]. First, blocks of a commercial open-cell polyurethane (PU) sponge (density about 20 kg m^{-3}) were cut in the form of planar strips by using a razor blade; then an appropriate, permanent curvature was imparted to these templates so that they could match the shape and size of the curved alumina substrates. Specifically, the PU sponge was ther-

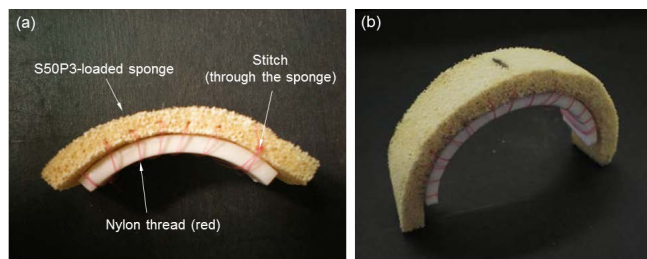


Figure 2: Joining of the glass-loaded sponge to the curved substrate by stitching: this method can be applied to (a) small-sized or (b) large-sized samples.

mally pre-formed by applying a heat treatment at 200°C for 1 h using the alumina curved substrate as a direct mould; afterwards, the curvature was permanently maintained by the polymeric template [19]. In order to take into account the volumetric shrinkage due to scaffold sintering, the dimensions (length and width) of the sponge strips were properly oversized of around 30% with respect to those of alumina curved substrates. The curved PU strips were then soaked into an aqueous suspension containing S50P3 powder sieved below 32 μm (slurry formulation: 30 wt.% glass, 6 wt.% PVA used as a binder, 64 wt.% distilled water) and compressed up to 60% in thickness for two times (the load was applied for 1 s first on the convex and then on the concave face of the sponge). This infiltration/compression cycle was repeated for three times followed by a final cycle of impregnation only. During each compression, the curvature of the sponge was temporarily cancelled and it became a planar strip again; after removing the compressive load, the curvature was successfully restored. After the end of the whole process, the glass-coated sponges were left to dry overnight under ambient conditions.

Porous S50P3 cuboids (side around 10 mm) were also produced, according to the same schedule processing, to characterize the new glass-derived scaffold from morphological, mechanical and bioactive viewpoints using a simplified cubic geometry.

The 3-layer construct schematically depicted in Fig. 1 was produced by joining SCNA-coated curved alumina samples and S50P3-loaded sponges together by stitching with a nylon thread (Fig. 2). Finally, the whole system was thermally-treated at 1000°C for 3 h (heating and cooling rates set at 5 and 10°C min⁻¹, respectively) to allow burning-out of the PU template and the nylon thread, as well as sintering of glass powders and the formation of alumina/interlayer and interlayer/trabecular coating stable interfaces.

2.4 Characterisation

Both as-cast S50P3 and S50P3-derived scaffolds (ground in powder) underwent wide-angle X-ray diffraction analysis (2θ within 10-70°) using a X'Pert diffractometer operating at 40 kV and 30 mA (Bragg-Brentano camera geometry with Cu K α incident radiation, incident wavelength $\lambda = 0.15405$ nm, step size $\Delta(2\theta) = 0.02^\circ$, fixed counting time of 1 s per step). Phase identification was performed by using X'Pert HighScore software equipped with PCPDFWIN database.

Differential thermal analysis (DTA) was carried out on 50 mg of glass powder by using a DTA7 Perkin-Elmer instrument (temperature range: 50-1300°C; heating rate: 20°C min⁻¹). Pure alumina powder (Sigma-Aldrich) was used as a reference material and for baseline determination. The characteristic temperatures of S50P3, *i.e.* glass transition temperature (T_g), onset crystallization temperature (T_x) and peak crystallization temperature (T_c), were assessed directly from the DTA plot.

The sintering process of a glass powder compact was monitored by hot-stage microscopy (HSM) (Expert System Solutions instrument) performed in air atmosphere to approximate the chemo-environmental conditions of the furnace chamber during the scaffold (trabecular coating) heat treatment. This analysis provides useful information for selecting the appropriate sintering temperature in order to obtain, at least ideally, scaffolds with well-densified trabeculae, high mechanical strength and adequate pore content for bone tissue engineering applications. HSM allows quantifying the shrinkage upon sintering by measuring the variation of specimen size during a controlled heating process (temperature range 50-1300°C and heating rate 20°C min⁻¹, consistently with DTA). The sample for HSM analysis was prepared by manually pressing the glass powder using a small cylindrical mould (base diameter ~1 mm, height ~3 mm). Sample shrinkage at different temperatures, $\Delta S_{glass,T}$ (%), was assumed as isotropic and was estimated as:

$$\Delta S_{glass,T} = \left(1 - \frac{A_T}{A_0}\right) \times 100 \quad (1)$$

where A_0 is the area of the sample silhouette at room temperature and A_T is the sample area at the temperature T .

S50P3 scaffolds were metal-coated and analysed from a morphological viewpoint by scanning electron microscopy (SEM, Philips 525 M; working voltage: 15 kV) to investigate the surface morphology and assess pore/strut size and shape.

The inner porous network was also non-destructively investigated by micro-computed tomography (micro-CT;

SkyScan 1174, Micro Photonics Inc.). Sample volume reconstruction and 3-D visualization were performed by making use of N-Recon and CT-Vox softwares, respectively.

The volumetric shrinkage of the scaffolds, $\Delta S_{scaffold}$ (%), due to the polymeric template removal and the glass softening-sintering, was calculated as

$$\Delta S_{scaffold} = \left(1 - \frac{V_s}{V_0}\right) \times 100 \quad (2)$$

where V_0 is the volume of the glass-impregnated sponge before sintering and V_s is the volume of the sintered scaffold.

The porosity content P (vol.%) was calculated by means of geometrical mass-volume measurements as

$$P = \left(1 - \frac{\rho_s}{\rho_b}\right) \times 100 \quad (3)$$

where ρ_b is the density of bulk material and ρ_s is the apparent density of the scaffold (mass/volume ratio).

The strength of the scaffolds was evaluated through crushing tests on 10 mm × 10 mm × 10 mm polished cuboids (Synthec 10/D apparatus, 5-kN cell load, cross-head speed set at 1 mm min⁻¹). The compressive failure stress, σ_c (MPa), was calculated as

$$\sigma_c = \frac{L_M}{A_R} \quad (4)$$

where L_M (N) is the maximum load registered during the test and A_R (mm²) is the resistant cross-sectional area.

The energy per unit volume W (J mm⁻³) absorbed by the scaffold till the breaking off is reached was defined as the energy necessary to deform a specimen from the unloaded condition to the failure strain ε_f and was calculated as the area under the stress-strain curve up to ε_f [20]:

$$W = \int_0^{\varepsilon_f} \sigma(\varepsilon) d\varepsilon \quad (5)$$

where the strain ε is the integration variable; the initial condition is $\sigma(\varepsilon = 0) = 0$ and the final state $\sigma(\varepsilon = \varepsilon_f) = \sigma_c$ (calculated from Eq. 4). The above-mentioned mechanical parameters were expressed as mean value ± standard deviation calculated on five samples.

In vitro tests were carried out by soaking the scaffolds in simulated body fluid (SBF) prepared according to Kokubo's protocol [21]. S50P3 porous cuboids (side around 10 mm) were soaked for 7 and 28 days in 30 ml of SBF maintained at 37°C in polyethylene bottles. Every 48 h the samples were extracted from the bottles, gently rinsed with some drops of distilled water and then soaked in 30 ml of new SBF. Periodic replacement of SBF is a common experimental practice to simulate fluid circulation in the human

body [14, 18] as the cation concentration in the solution progressively decreases during the experiment as a result of changes in the sample surface chemistry.

The pH of the solution was monitored daily. At the end of the experiment, the samples were left to dry at room temperature and then investigated by SEM and energy dispersive spectroscopy (EDS, Philips EDAX 9100) for compositional analysis. Mass loss and compressive strength of S50P3 scaffolds soaked for 1 month in SBF were also assessed.

Selected samples from *in vitro* tests and complete curved samples were embedded in epoxy resin (EpoFix, Struers), cut with a diamond blade (Accutom 5 cutting machine, Struers) and polished using #600 to #4000 SiC grit paper; the obtained cross-sections were metal-coated and then analysed by SEM in back-scattering mode to enhance the discrimination among the different layers.

3 Results

A comprehensive characterization of SCNA has been reported elsewhere by the authors [14, 15]. The characteristic temperatures of SCNA are $T_g = 690^\circ\text{C}$, $T_x = 820^\circ\text{C}$ and $T_c = 856^\circ\text{C}$. The thermal treatment applied in this work (1000°C for 3 h) induced the development of one crystalline phase identified as wollastonite (CaSiO₃) [14, 15]. Therefore, SCNA crystallizes forming a glass-ceramic interlayer.

In this work, sintering and crystallization of the new glass S50P3 were investigated for the first time. While designing glass composition, we analytically estimated the coefficient of thermal expansion (CTE) by making use of the program Priven2000 (SciGlass software), in order to avoid a too high mismatch with the CTE of the interlayer (Table 1).

The characteristic temperatures of S50P3, assessed by DTA and marked in Fig. 3a, are $T_g = 620^\circ\text{C}$, $T_x = 730^\circ\text{C}$ and $T_c = 810^\circ\text{C}$. A quantitative evaluation of S50P3 shrinkage depending on the sintering temperature can be derived from the curve plotted in Fig. 3b, showing that S50P3 exhibits a 1-step densification behaviour. Specifically, densification begins at $T_g \approx T_{FS}$ (first shrinkage) and is fully completed when crystallization starts at $T_x \approx T_{MS}$ (maximum shrinkage). We estimated that the shrinkage up to T_{MS} was around 37%. The sintering temperature for producing S50P3 scaffolds (1000°C) was chosen slightly after the end of the plateau following the maximum densification.

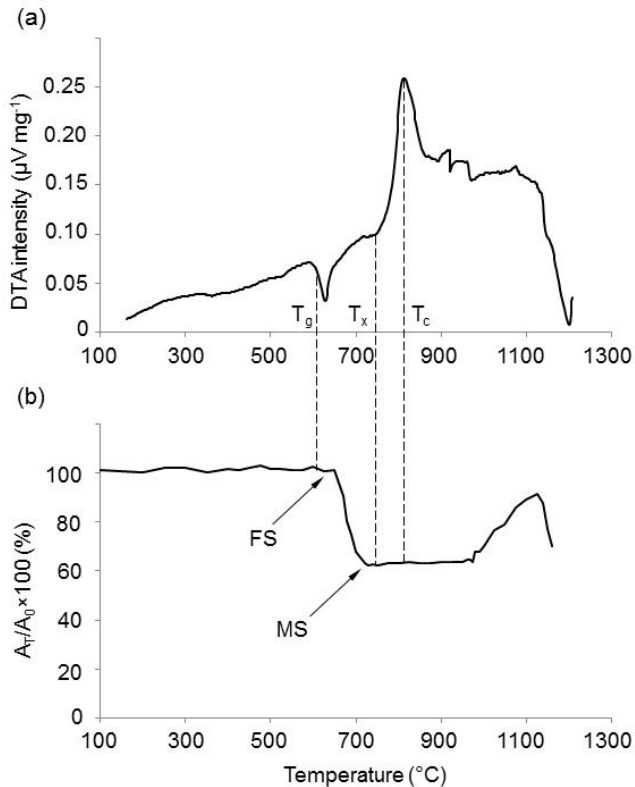


Figure 3: Thermal analyses performed on S50P3 glass: (a) differential thermal analysis (DTA) and (b) hot-stage microscopy (HSM).

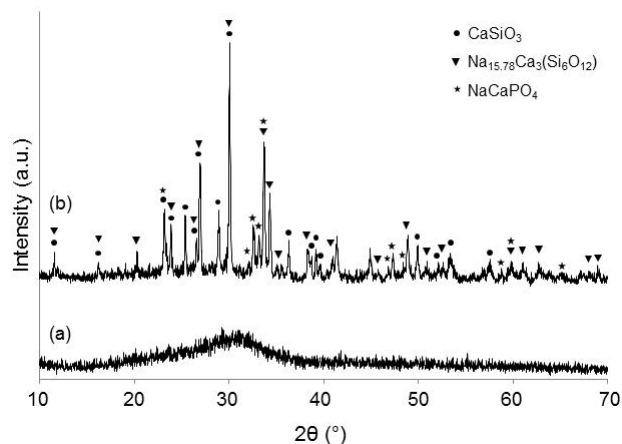


Figure 4: XRD pattern of (a) as-cast S50P3 and (b) S50P3 scaffold produced by thermal treatment at 1000°C for 3 h and subsequently ground in powder.

As-poured S50P3 is a completely amorphous material (glass), as demonstrated by the broad halo in the XRD pattern shown in Fig. 4a. Three crystalline phases, identified as wollastonite (CaSiO_3 , code 00-027-0088), calcium-sodium silicate ($\text{Na}_{15.78}\text{Ca}_3(\text{Si}_6\text{O}_{12})$, code 01-078-1650) and rhenanite (NaCaPO_4 , code 00-029-1193) were detected in

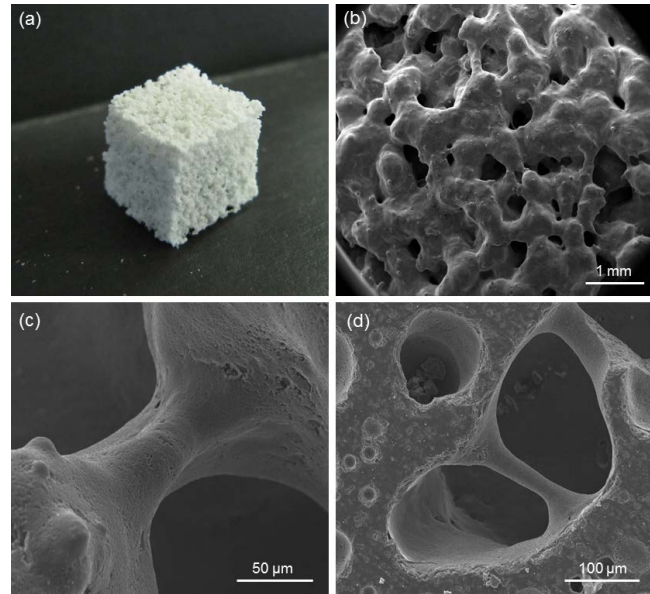


Figure 5: Morphological investigation of S50P3 scaffolds: (a) camera picture of a typical porous cuboid (side around 10 mm); SEM micrographs of (b) scaffold surface (magnification 50 \times), (c) a well-sintered trabecula (1200 \times) and (d) cross-section showing the interconnectivity of the pores (600 \times).

the material sintered at 1000°C for 3 h (Fig. 4b). Therefore, it should be taken into account that, after the thermal treatment, S50P3 was converted into a glass-ceramic material; however, for purpose of simplicity, hereafter we will use expressions such as “S50P3 scaffold” without any further specification.

A typical S50P3 porous cuboid is shown in Fig. 5a. The volumetric shrinkage was $65.9 \pm 2.2\%$, and the total porosity was $62.1 \pm 2.4 \text{ vol.}\%$. In both cases, the low values of standard deviation demonstrate the good reproducibility of the samples. The SEM micrographs reported in Fig. 5b-d show that an excellent densification of the scaffold struts was achieved, with a 3-D pore architecture that closely reproduces the trabecular structure of cancellous bone. Fig. 5d suggests that the pores are interconnected, with size above $100 \mu\text{m}$, thus allowing bone cells to colonize the implant and bone tissue to regenerate inside the scaffold in an *in vivo* scenario.

The scaffold is strong enough to be cut neatly with a diamond blade (Fig. 5d) without any apparent damage to the structure. The compressive strength of S50P3 cubic scaffolds was $19.1 \pm 2.7 \text{ MPa}$, and the mean fracture energy (assessed from the stress-strain curves) was $6.5 \times 10^{-4} \text{ J mm}^{-3}$.

A typical example of compressive stress-strain curve for S50P3 scaffolds is reported in Fig. 6. The curve exhibits a multi-peak profile, which is peculiar of cellular ceramics [22]. The curve has a positive slope up to a first peak,

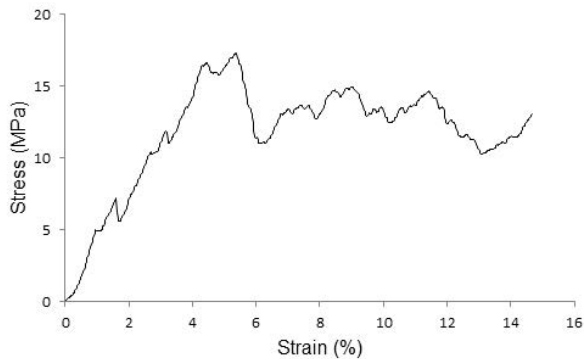


Figure 6: Typical stress-strain curve for S50P3 cubic scaffolds.

then the thinnest trabeculae begin to crack causing an apparent stress drop (negative slope). However, the scaffold is still able to withstand higher loads and, therefore, the stress rises again. The repetition of this behaviour produces a jagged stress-strain curve while the progressive cracking of scaffold struts occurs.

After soaking for 7 days in SBF, the scaffold struts were coated by a well-distinguishable layer of a newly formed phase, which also grew on the walls of the inner pores of the scaffold (Figs. 7a and 7b). Compositional analysis reveals that this layer is rich in Ca and P (Fig. 7d). After soaking for 1 month in SBF, the thickness of this CaP layer seems to be higher compared to the previous time point (around 20 vs. 10 μm). The peak of Si, associated to the presence of a silica gel layer after 7 days in SBF (consistently with the mechanism of bioactivity of silicate glasses [1]), is no longer detectable after 1 month of soaking (Fig. 7f). At the end of the experiment, the Ca/P ratio was equal to 1.2 at.%, which is typical of Ca-deficient hydroxyapatite (HA) formed on bioactive glasses. The increment of the pH of the solution is moderate; pH reaches values around 7.70 by the first 10 days of soaking and then progressively decreases.

Low tendency of S50P3 scaffolds to dissolve upon soaking in biological media was further confirmed by mass loss assessment. After 1-month immersion, mass loss of about 2% was registered, which involved a very moderate decrease of the compressive strength compared to that of untreated samples (-10%).

Complete curved samples were produced by stitching (Fig. 2) followed by thermal treatment. From a qualitative viewpoint, good joining at the alumina/SCNA interlayer and SCNA interlayer/S50P3 trabecular coating interfaces was observed (Fig. 8). Sintered curved samples could be manipulated without any particular problem, as the trabecular coating seemed to be tightly attached to the

SCNA/alumina substrate lying underneath. Fig. 8d shows that the interlayer/trabecular coating interface was not distinguishable in correspondence of the contact areas between SCNA and S50P3, which confirms the good quality of the joining in these points. A few isolated defects, visible in Figs. 8a and 8b, are due to the stitching thread which created small perforations through the glass-loaded sponge, resulting in full-thickness holes and local crumbling of the trabecular coating upon heat treatment. Small closed pores visible in the trabecular coating are due to gas development associated to polymer sponge burn-off. The presence of closed pores also in the interlayer is due to PVA removal and air entrapment during the airbrush spraying process, as already observed elsewhere [12]. Micro-CT investigations revealed that a trabecular coating with quite homogeneous thickness (around 2 mm) can be successfully produced with the method proposed (Figs. 9a and 9b). The porous coating exhibited a continuous 3-D trabecular-like structure, which is very close to that of cancellous bone (Fig. 9c). Micro-CT analysis, performed in a 3-D space, is complementary to SEM investigation that provides information on a single 2-D cross-section of the sample. Fig. 9c puts in evidence the high interconnectivity of the trabecular coating macropores, which is a key requirement to allow bone cells to colonize the implant *in vivo* and the new bone to grow inside the pores.

4 Discussion

The composition of the new biomedical glass S50P3 was designed starting from that of the parent glass SCNA (Table 1), which was widely studied by the authors for biomedical applications [12, 14, 15, 19]. Our aim was to obtain a material with good mechanical and bioactive properties, while SCNA (in its both glassy and glass-ceramic forms) is mechanically strong but just weakly bioactive. Therefore, we decreased the content of silica (a dramatic decrease of the bioactivity kinetics was observed when glass composition exceeds 53 mol.% of silica [23]) and alumina (the presence of which is known to stabilize the glass network, thereby decreasing surface reactivity [24]), and increased the content of Na_2O (Na^+ ions are known to play a key role in the early stages of the bioactivity mechanism in silicate glasses [1]). MgO was introduced because of the beneficial effect of magnesium in stimulating osteoblast activity [25]. P_2O_5 was useful on one hand to further improve glass bioactivity interrupting locally the silica network and, accordingly, increasing glass reactivity and, on

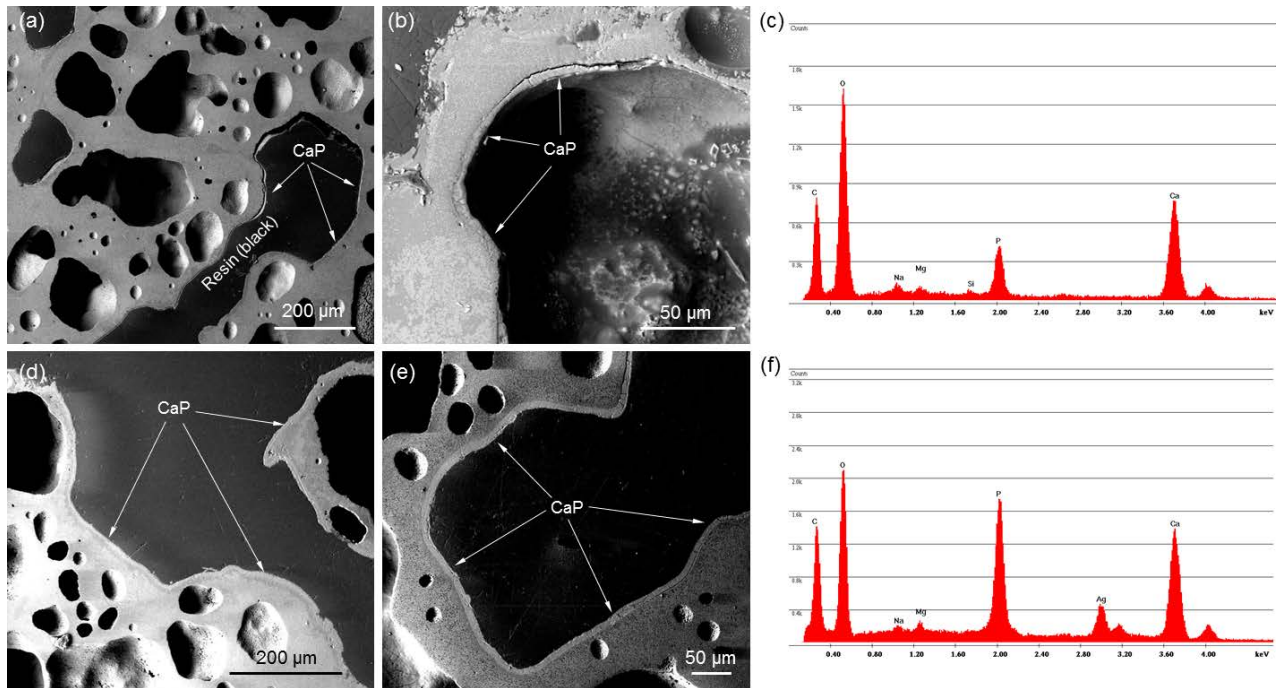


Figure 7: *In vitro* bioactivity of S50P3 scaffolds after soaking in SBF for (a-c) 7 days and (d-f) 28 days. SEM micrographs, acquired in back-scattering mode, refer to polished cross-sections of the samples embedded in epoxy resin; the magnifications are (a) 300×, (b) 1300×, (d) 400×, (e) 500×. EDS patterns in (c,f) refer to the newly formed layer on the scaffold struts marked in the SEM pictures (the peak of Ag is due to the metal costing needed for the analysis; the peak of C is attributable to resin-related boundary effect).

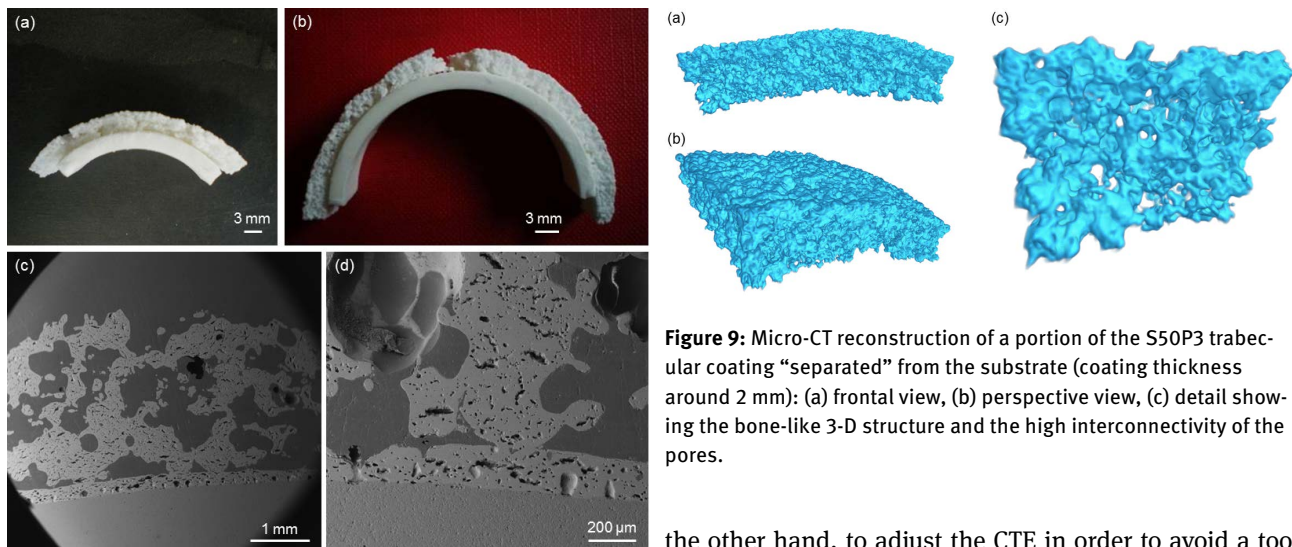


Figure 8: Complete curved samples (alumina substrate + SCNA interlayer + S50P3 trabecular coating) after sintering at 1000°C for 3 h: camera pictures of (a) small-sized and (b) large-sized samples; (c) SEM micrograph (back-scattering mode) of a polished cross-section after embedding the sample in epoxy resin (50×) and (d) detail of a contact area between interlayer and trabecular coating (200×).

Figure 9: Micro-CT reconstruction of a portion of the S50P3 trabecular coating “separated” from the substrate (coating thickness around 2 mm): (a) frontal view, (b) perspective view, (c) detail showing the bone-like 3-D structure and the high interconnectivity of the pores.

the other hand, to adjust the CTE in order to avoid a too high mismatch with the CTE of SCNA.

Following a strategy adopted in previous works [14, 15] and also proposed by other authors [26], we inserted a “bond coat” (SCNA-derived interlayer) having intermediate CTE between top layer (S50P3 trabecular coating) and alumina substrate (CTE around $8.5 \times 10^{-6} \text{ °C}^{-1}$) in order to overcome CTE mismatch problems.

Upon thermal treatment at 1000°C for 3 h, SCNA and S50P3 partially crystallize giving glass-ceramic ma-

materials. Wollastonite, the major crystalline phase developed in both SCNA interlayer [14, 15] and S50P3 scaffolds (Fig. 4b), is known to be highly biocompatible [27]. Rhenanite (Fig. 4b) is not only biocompatible [28] but is also known to transform into HA after reacting with water, thus being a nucleation precursor for HA formation [29]. Hence, no problems of possible cytotoxicity associated to the types of crystalline phases contained in the interlayer and scaffold (trabecular coating) materials are foreseen.

We found the sponge replication a highly suitable method to process S50P3 in the form of strong, porous scaffolds with 3-D trabecular architecture that closely mimicked that of cancellous bone (Fig. 5). Total porosity (around 62 vol.%) and pore size (large macropores above 100 μm) were in the ranges usually recommended for bone tissue engineering scaffolds [30].

The compressive strength of S50P3 scaffolds (around 19 MPa) is above the standard reference range usually considered for cancellous bone (2-12 MPa [1]) as well as most of foam-like scaffolds with a comparable pore content reported in the literature [31, 32]. This can be attributable to the higher silica content and to the presence of a small amount of alumina as an intermediate oxide, which is known to have a strengthening effect on the glass network. The high compressive strength suggests the suitability of S50P3 scaffolds as trabecular coatings for load-bearing prosthetic applications. The fracture energy of S50P3 scaffolds (around $6.5 \times 10^{-4} \text{ J mm}^{-3}$) is comparable to that assessed for SCNA scaffolds with the same porosity [33], but is significantly higher (more than one order of magnitude) than that of HA [34] and phosphate glass scaffolds [35] reported in the literature.

The good *in vitro* bioactivity of S50P3 scaffolds is demonstrated by the formation of an apatite-like layer on the pore struts (Fig. 7), which is a sort of precondition so that a stable interfacial bond to bone may develop *in vivo* [23]. Furthermore, the growth of apatite on the struts of the inner pores of the scaffold represents an indirect evidence of the high pore interconnectivity, which is a crucial feature for porous implants intended to biointegrate with bone. Mild increase of the pH of SBF (7.70) due to ion-exchange phenomena with the bioactive glass-ceramic surface could even be beneficial *in vivo*, as moderate alkaline conditions (pH up to 7.8) can stimulate osteoblast activity [36].

The decrease of compressive strength due to minimal *in vitro* dissolution of S50P3 scaffolds is very moderate, which suggests adequate maintenance of integrity upon prolonged contact with biological fluids.

In a previous work [14] we also assessed the mass loss of SCNA glass-ceramic scaffolds after long-term soaking in

SBF. After soaking for 3 months in SBF, the mass loss of SCNA scaffolds was about 3%. This confirms the high stability of the material, characterized by a very moderate solubility in SBF.

The very low tendency of S50P3- and SCNA-based glass-ceramics to dissolve in aqueous media can be attributable to the high chemical stability of the alumina-containing glassy phases. Therefore, no problems of durability and overall integrity of the 3-layer device are foreseen after implantation. On the other hand, it cannot be ignored that *in vitro* results are indeed useful but offer, unavoidably, only an estimate of what happens in an *in vivo* scenario. For example Liu *et al.* [37] implanted 13-93 scaffolds in rats and observed that the brittle response of as-such and *in vitro* samples changed to an elasto-plastic behaviour after 2-4 weeks *in vivo*. This is due to the fact that the cells adherent on the trabecular coating, the newly formed bone and the scaffold itself create a “living” bio-composite *in situ*.

Release of Mg^{2+} ions from the glassy phase of S50P3 trabecular coating is expected to stimulate osteoblast activity *in vivo* and, accordingly, new bone formation [25].

In summary, the novel glass S50P3 was designed to give good mechanical and bioactive properties. Both scopes were achieved, as the S50P3 (glass-ceramic) scaffold was strong and the HA layer formation upon soaking in SBF suggests that the parent S50P3 glass actually gives a bioactive glass-ceramic, thus the compositional design was successful. The sponge replication technique combined with stitching (Fig. 2) represents a novel, creative and interesting approach to produce bioactive glass-derived trabecular coatings on curved substrates. However, the method has to be optimized to solve some shortcomings, such as the low number of contact areas between interlayer and porous coating and the lack of full integrity of the trabecular layer – especially for large sample sizes (Fig. 8).

5 Conclusions

In the present work, we proposed to make use of glass-derived scaffolds as trabecular coatings on curved alumina substrates, with the aim of inducing biological fixation of bioceramic prostheses to bone. The feasibility of bone-like trabecular coatings in a curved geometry using the sponge replication method was successfully demonstrated. The trabecular coating showed to be bioactive *in vitro* and strong enough to be safely manipulated without any apparent damage. The results presented in this work

provide an important stimulus for the research in the field of bioceramic implants; the next step of this research will be extending these achievements to a semi-spherical configuration typical of the real acetabular component of hip joint prosthesis.

Acknowledgement: The research leading to these results has received funding from the EU Seventh Framework Programme (FP7/2007-2013) under grant agreement no. 286548 (project MATCH).

References

- [1] Hench L.L., Bioceramics, *J. Am. Ceram. Soc.*, 1998, 81, 1705-1728.
- [2] Hench L.L., Chronology of Bioactive Glass Development and Clinical Applications, *N. J. Glass Ceram.*, 2013, 3, 67-73.
- [3] Rahaman M.N., Yao A., Sonny Bal B., Garino J.P., Ries N.D., Ceramics for Prosthetic Hip and Knee Joint Replacement, *J. Am. Ceram. Soc.*, 2007, 90, 1965-1988.
- [4] Marshall D.A., Pykerman K., Werle J., Lorenzetti D., Wasylak T., Noseworthy T., *et al.*, Hip Resurfacing Versus Total Hip Arthroplasty: A Systematic Review Comparing Standardized Outcomes, *Clin. Orthop. Relat. Res.*, 2014, 472, 2217-2230.
- [5] Verné E., Bioactive glass and glass-ceramic coatings, In: Jones J.R., Clare A.G. (Eds.), *Bio-glasses: an introduction*, Wiley, Chichester (UK), 2012.
- [6] Vitale Brovarone C., Verné E., Krajewski A., Ravaglioli A., Graded Coatings on Ceramic Substrates for Biomedical Applications, *J. Eur. Ceram. Soc.*, 2001, 21, 2855-2862.
- [7] Lee T.M., Chang E., Wang B.C., Yang C.Y., Characteristics of Plasma-Sprayed Bioactive Glass Coatings on Ti-6Al-4V Alloy: An in Vitro Study, *Surf. Coatings Technol.*, 1996, 79, 170-177.
- [8] Wang X., Li X., Onuma K., Ito A., Sogo Y., Kosuge K., *et al.*, Mesoporous Bioactive Glass Coatings on Stainless Steel for Enhanced Cell Activity, Cytoskeletal Organization and AsMg Immobilization, *J. Mater. Chem.*, 2010, 20, 6437-6445.
- [9] Mardare C.C., Mardare A.I., Fernandes J.R.F., Joanni E., Pina S.C.A., Fernandes M.H.V., *et al.*, Deposition of Bioactive Glass-Ceramic Thin Films by RF Magnetron Sputtering, *J. Eur. Ceram. Soc.* 2003, 23, 1027-1030.
- [10] Boccaccini A.R., Keim S., Ma R., Li Y., Zhitomirsky I., Electrophoretic Deposition of Biomaterials, *J. R. Soc. Interface*, 2010, 7, S581-S613.
- [11] Fiorilli S., Baino F., Cauda V., Crepaldi M., Vitale-Brovarone C., Demarchi D., *et al.*, Electrophoretic Deposition of Mesoporous Bioactive Glass on Glass-Ceramic Foam Scaffolds for Bone Tissue Engineering, *J. Mater. Sci.: Mater. Med.*, 2015, 26, art.21, pp.12.
- [12] Baino F., Vitale-Brovarone C., Feasibility of Glass-Ceramic Coatings on Alumina Prosthetic Implants by Airbrush Spraying Method, *Ceram. Int.*, 2015, 41, 2150-2159.
- [13] Verné E., Vitale-Brovarone C., Robiglio L., Baino F., Single-piece ceramic prosthesis elements, Patent no. EP2152328.
- [14] Vitale-Brovarone C., Baino F., Tallia F., Gervasio C., Verné E., Bioactive Glass-Derived Trabecular Coating: A Smart Solution for Enhancing Osteointegration of Prosthetic Elements, *J. Mater. Sci. Mater. Med.*, 2012, 23, 2369-2380.
- [15] Chen Q., Baino F., Pugno N.M., Vitale-Brovarone C., Bonding Strength of Glass-Ceramic Trabecular-Like Coatings to Ceramic Substrates for Prosthetic Applications, *Mater. Sci. Eng. C*, 2013, 33, 1530-1538.
- [16] Chen Q.Z., Thompson I.D., Boccaccini A.R., 45S5 Bioglass®-Derived Glass-Ceramic Scaffolds for Bone Tissue Engineering, *Biomaterials*, 2006, 27, 2414-2425.
- [17] Vitale-Brovarone C., Verné E., Robiglio L., Appendino P., Bassi F., Martinasso G., *et al.*, Development of Glass-Ceramic Scaffolds for Bone Tissue Engineering: Characterisation, Proliferation of Human Osteoblasts and Nodule Formation, *Acta Biomater.*, 2007, 3, 199-208.
- [18] Vitale-Brovarone C., Baino F., Verné E., High Strength Bioactive Glass-Ceramic Scaffolds for Bone Regeneration, *J. Mater. Sci. Mater. Med.*, 2009, 20, 643-653.
- [19] Baino F., Tallia F., Novajra G., Minguella J., Montealegre M.A., Korkusuz F., *et al.*, Novel Bone-Like Porous Glass Coatings on Al₂O₃ Prosthetic Substrates, *Key Eng. Mater.*, 2015, 631, 236-240.
- [20] Kenesei P., Kadar C., Rajkovits Z., Lendvai J., The Influence of Cell-Size Distribution on the Plastic Deformation in Metal Foams, *Scripta Mater.*, 2004, 50, 295-300.
- [21] Kokubo T., Takadama H., How Useful is SBF in Predicting in Vivo Bone Bioactivity?, *Biomaterials*, 2006, 27, 2907-2915.
- [22] Rice R., Mechanical Properties, In: Schauer H., Colombo P., (Eds.), *Cellular ceramics: structure, manufacturing, properties and applications*, Wiley, New York, 2005.
- [23] Hench L.L., Bioactive Ceramics, *Ann. N.Y. Acad. Sci.*, 1988, 523, 54-57.
- [24] Andersson O.H., Liu G., Karlsson K.H., Juhanoja J., In Vivo Behaviour of Glasses in the SiO₂-Na₂O-CaO-P₂O₅-Al₂O₃-B₂O₃ System, *J. Mater. Sci.: Mater. Med.*, 1990, 1, 219-227.
- [25] Vormann J., Magnesium: Nutrition and Metabolism, *Mol. Aspects Med.*, 2003, 24, 27-37.
- [26] Kim C.Y., Lee J.W., Surface Bio-Modification of Titanium Implants by an Enamel Process, *J. Ceram. Process. Res.*, 2005, 6, 338-344.
- [27] Kokubo T., Ito S., Sakka S., Yamamuro T., Formation of a High Strength Bioactive Glass-Ceramic in the System MgO-CaO-SiO₂-P₂O₅, *J. Mater. Sci.*, 1986, 21, 536-540.
- [28] Suchanek W., Yashima M., Kakihana M., Yoshimura M., Rhenanite (β -NaCaPO₄) as Weak Interphase for Hydroxyapatite Ceramics, *J. Eur. Ceram. Soc.*, 1998, 18, 1923-1929.
- [29] Jalota S., Bhaduri S.B., Tas A.C., A New Rhenanite (β -NaCaPO₄) and Hydroxyapatite Biphasic Biomaterial for Skeletal Repair, *J. Biomed. Mater. Res. B*, 2007, 80, 304-316.
- [30] Karageorgiou V., Kaplan D., Porosity of 3D Biomaterial Scaffolds and Osteogenesis, *Biomaterials*, 2005, 26, 5474-5491.
- [31] Fu Q., Rahaman M.N., Bal B.S., Brown R.F., Day D.E., Mechanical and in Vitro performance of 13-93 Bioactive Glass Scaffolds Prepared by a Polymer Foam Replication Technique, *Acta Biomater.*, 2008, 4, 1854-1864.
- [32] Baino F., Ferraris M., Bretcanu O., Verné E., Vitale-Brovarone C., Optimization of Composition, Structure and Mechanical Strength of Bioactive Glass-Ceramic Scaffolds for Bone Substitution, *J. Biomater. Appl.*, 2013, 27, 872-890.
- [33] Baino F., Vitale-Brovarone C., Mechanical Properties and Reliability of Glass-Ceramic Foam Scaffolds for Bone Repair, *Mater.*

- Lett., 2014, 118, 27-30.
- [34] Kim H.W., Knowles J.C., Kim H.E., Hydroxyapatite Porous Scaffolds Engineered with Biological Polymer Hybrid Coating for Antibiotic Vancomycin Release, *J. Mater. Sci. Mater. Med.*, 2005, 16, 189-195.
- [35] Vitale-Brovarone C., Ciapetti G., Leonardi E., Baldini N., Bretcanu O., Verné E., *et al.*, Resorbable Glass-Ceramic Phosphate-Based Scaffolds for Bone Tissue Engineering: Synthesis, Properties and in Vitro Effects on Human Marrow Stromal Cells, *J. Biomater. Appl.*, 2011, 26, 465-489.
- [36] Kaysinger K.K., Ramp W.K., Extracellular pH Modulates the Activity of Cultured Human Osteoblasts, *J. Cell. Biochem.*, 1998, 68, 83-89.
- [37] Liu X., Rahaman M.N., Hilmas G.E., Sonny Bal B., Mechanical Properties of Bioactive Glass (13-93) Scaffolds Fabricated by Robotic Deposition for Structural Bone Repair, *Acta Biomater.*, 2013, 9, 7025-7034.